

# Binary and Multiple O-Type Stars in the Cas OB6 Association

Todd C. Hillwig<sup>1,2</sup>, Douglas R. Gies<sup>1</sup>, William G. Bagnuolo, Jr., Wenjin Huang<sup>1</sup>,  
M. Virginia McSwain<sup>1,3,4</sup>, and David W. Wingert<sup>1</sup>

*Center for High Angular Resolution Astronomy and  
Department of Physics and Astronomy, Georgia State University, P. O. Box 4106, Atlanta,  
GA 30302-4106; todd.hillwig@valpo.edu, gies@chara.gsu.edu, bagnuolo@chara.gsu.edu,  
huang@chara.gsu.edu, mcswain@astro.yale.edu, wingert@chara.gsu.edu*

## ABSTRACT

We present the results of time-resolved spectroscopy of 13 O-type stars in the Cas OB6 stellar association. We conducted a survey for radial velocity variability in search of binary systems, which are expected to be plentiful in young OB associations. Here we report the discovery of two new single-lined binaries, and we present new orbital elements for three double-lined binaries (including one in the multiple star system HD 17505). One of the double-lined systems is the eclipsing binary system DN Cas, and we present a preliminary light curve analysis that yields the system inclination, masses, and radii. We compare the spectra of the single stars and the individual components of the binary stars with model synthetic spectra to estimate the stellar effective temperatures, gravities, and projected rotational velocities. We also make fits of the spectral energy distributions to derive  $E(B - V)$ ,  $R = A_V/E(B - V)$ , and angular diameter. A distance of 1.9 kpc yields radii that are consistent with evolutionary models. We find that 7 of 14 systems with spectroscopic data are probable binaries, consistent with the high binary frequency found for other massive stars in clusters and associations.

---

<sup>1</sup>Visiting Astronomer, Kitt Peak National Observatory, National Optical Astronomical Observatory, which is operated by the Association of Universities for Research in Astronomy, Inc. (AURA) under cooperative agreement with the National Science Foundation.

<sup>2</sup>Current address: Department of Physics and Astronomy, Valparaiso University, Valparaiso, IN 46383

<sup>3</sup>Current address: Department of Astronomy, Yale University, P. O. Box 208101, New Haven, CT 06520-8101

<sup>4</sup>NSF Astronomy and Astrophysics Postdoctoral Fellow

*Subject headings:* binaries: close — stars: early-type — stars: individual (DN Cas, BD+60°497, HD 17505, HD 17520, BD+60°594) — open clusters and associations: individual (Cas OB6, IC 1805, IC 1848)

## 1. Introduction

The frequency of spectroscopic binaries (SBs) in star forming regions has been a topic of interest for many years. Mason et al. (1998) review the fraction of binary systems found among O stars in clusters/associations, the field, and runaway systems. The results from their large survey agree with previous studies (e.g. Garmany, Conti, & Massey 1980; Levato et al. 1991) and indicate that a large fraction of O stars in clusters and associations are binaries while fewer field stars show multiplicity and very few runaway stars have companions. The values from Mason et al. (1998) are broken down into spectroscopic and resolved binaries. For O stars in clusters and associations they give a total of 75% as binaries; 61% of the binaries are spectroscopic and 41% are resolved (with some obvious overlap). The spectroscopic binary group includes, however, a significant number of cases labeled as SB1? or SB2? (systems suspected of radial velocity variability or showing double lines), so the fraction of confirmed spectroscopic binaries is then 34% among O stars in clusters and associations.

We have conducted a radial velocity survey of O-type stars in the Cas OB6 stellar association in search of spectroscopic binary systems. The Cas OB6 region is one of the largest complexes in the Perseus arm of the Galaxy and is located at a distance of about 2.3 kpc (Garmany & Stencel 1992; Massey, Johnson, & DeGioia-Eastwood 1995; Foster & Routledge 2003). The warm dust and ionized gas in this region extends over 150 pc along the arm and is dominated by the W3/W4/W5 chain of H II regions and the HB3 supernova remnant (Carpenter, Heyer, & Snell 2000; Terebey et al. 2003). The open cluster IC 1805 (OCL 352 = Melotte 15) is situated at the western end in the W4 region and contains 8 O-type stars (Massey et al. 1995). The three brightest of these, HD 15558, 15570, and 15629, are probably the ionization source that powers the blowout of gas in the Galactic chimney (Normandeau, Taylor, & Dewdney 1996; Terebey et al. 2003) and the emission arc above W4 (Reynolds, Sterling, & Haffner 2001). The open cluster IC 1848 (OCL 364) is found in the eastern part of the association in the W5 region. Its primary source of ionizing flux is the multiple O-star system HD 17505 (Stickland & Lloyd 2001). In addition to these two clusters, Carpenter et al. (2000) find evidence of 19 other young clusters that are still embedded in their primordial clouds.

Our knowledge of the binary star population among the young, massive stars of Cas OB6 is quite limited at present. There are a number of radial velocity investigations of the sample but the overall small number of measurements has made the detection of binary stars difficult (Hayford 1932; Underhill 1967; Ishida 1970; Conti, Leep, & Lorre 1977; Liu, Janes, & Bania 1989, 1991; Rauw & De Becker 2004). Spectroscopic orbits are available for only three systems, HD 15558 (Garmany & Massey 1981), HD 16429 (McSwain 2003), and BD+60°497 (Rauw & De Becker 2004), while a fourth star, BD+60°470 = DN Cas, is a known eclipsing binary (Frazier & Hall 1974). However, results for O-stars in other clusters and associations suggest that many more binaries may exist (Mason et al. 1998; Garcia & Mermilliod 2001). It is important to determine the extent of the binary star population in Cas OB6 in order to estimate accurately the ionizing flux of the key O-type stars and to assess the role of gravitational encounters with binary stars that might lead to ejection of runaway stars (Gies & Bolton 1986; Hoogerwerf, de Bruijne, & de Zeeuw 2001).

Here we present a reconnaissance of the radial velocity variations observed in 13 bright stars in Cas OB6 that we obtained over a 5 night run with the KPNO 4 m Mayall telescope in 2003 October. We also present the first radial velocity study of the eclipsing binary system DN Cas, which we combine with published photometry to determine the component masses. We discuss our observations and reduction techniques in §2. The radial velocity measurements and the derivation of orbital elements are summarized in §3. We use a tomography algorithm to separate the spectra of the binary star components, and we describe a comparison of the stellar spectra with model spectra in §4 that we use to estimate the basic stellar parameters. We examine in §5 the spectral energy distributions to determine reddening, ratio of total-to-selective extinction, and angular size for each target, and we discuss the probable distance to Cas OB6. Details about the individual objects follow in §6. Finally we summarize in §7 our derived fraction of multiple and single systems for Cas OB6 in the context of past results.

## 2. Spectroscopic Observations and Reductions

The blue spectra were obtained with the RC spectrograph at the Mayall 4 m telescope at Kitt Peak National Observatory from 2003 September 30 through 2003 October 4. The spectra were made with the BL 380 grating (1200 grooves  $\text{mm}^{-1}$ , blazed at 4500 Å in second order) using a BG39 order sorting filter. The detector was the T2KB CCD, a  $2048 \times 2048$  device with 24  $\mu\text{m}$  square pixels. The spectra recorded wavelengths between 4180 and 4940 Å, although internal vignetting occurs for wavelengths red-ward of about 4800 Å. The reciprocal dispersion of the spectra is approximately  $0.37 \text{ Å pixel}^{-1}$ , and the resolving power

is  $R = \lambda/\Delta\lambda = 5700$ . Exposure times were usually a few minutes in length, and each stellar spectrum was preceded and followed by a He-Ne-Ar lamp exposure for careful wavelength calibration. Most of the resulting spectra have a signal-to-noise ratio in excess of  $100 \text{ pixel}^{-1}$ . We usually obtained at least two spectra of each target on each of five consecutive nights. We also made numerous bias and flat field frames each night. A list of the names of targets appears in Table 1.

We also obtained an additional 32 spectra of HD 17505A with the KPNO 0.9 m Coude Feed telescope in runs in 2000 October and 2000 December (Boyajian et al. 2005). The spectra were made with the long collimator, grating B (in second order with order sorting filter OG550), camera 5, and a Ford  $3072 \times 1024$  CCD (F3KB) detector. This arrangement produced a resolving power,  $R = \lambda/\Delta\lambda = 9530$ , and covered a range of  $829 \text{ \AA}$  around  $H\alpha$ . Exposure times were 10 – 15 minutes, and the resulting spectra have a  $S/N = 200$  in the continuum. We also observed the rapidly rotating A-type star,  $\zeta \text{ Aql}$ , which we used for removal of atmospheric water vapor lines. Each set of observations was accompanied by numerous bias, flat field, and Th Ar comparison lamp calibration frames.

The spectra were reduced using standard routines in IRAF<sup>4</sup> to create continuum rectified versions of each spectrum. Then all the spectra of a given target were transformed to a common heliocentric frame in  $\log \lambda$  form and collected in a spectrum matrix of wavelength and time for subsequent analysis. The rectification of the vignetted portion of the spectrum was generally problem-free, so we used the entire spectral range in the following analysis.

### 3. Radial Velocities and Orbital Elements

We found that the spectra of 10 of the 13 targets were composed of one set of spectral lines, and for these targets we obtained radial velocities by finding the extremum point of the cross-correlation of each spectrum with a spectrum template (omitting those spectral regions containing interstellar features). We initially obtained velocities using the first spectrum as the template, and then we shifted each spectrum to the reference frame of the first spectrum and co-added all the spectra to form a high S/N template. The final relative velocities were then found by cross-correlation with this high S/N template spectrum. These relative velocities were then transformed to absolute velocity by adding the velocity measured in the template spectrum by fitting parabolae to the lower portions of selected spectral

---

<sup>4</sup>IRAF is distributed by the National Optical Astronomical Observatory, which is operated by the Association of Universities for Research in Astronomy, Inc. (AURA), under cooperative agreement with the National Science Foundation.

lines. Rest wavelengths were taken from the list of Bolton & Rogers (1978). The final velocities for these 10 stars are listed in Table 2 (which appears only in the electronic version), and the mean velocity  $\langle V_r \rangle$  for each star is given in column 3 of Table 1. Note that the adopted absolute velocity of the template spectrum depends critically on what subset of lines is measured because of the presence of significant line-to-line velocity differences. These differences mainly result from line formation at differing heights in an expanding stellar atmosphere (Hutchings 1976; Bohannan & Garmany 1978; Gies & Bolton 1986). We generally selected high excitation lines that form deep in the atmosphere where the outflow velocity is smallest (see discussion of the individual targets in §6). We list in column 4 of Table 1  $\sigma(l-l)$ , the standard deviation of the measured velocity among different lines in the template spectrum.

We used a version of the statistical  $F$ -test to determine if a star was a velocity variable object. Since we usually obtained at least two spectra every night of each object and since we do not expect large variations in velocity over the time span of a few hours, we estimated the average measurement error from the mean of the absolute value of the differences within a night divided by  $\sqrt{2}$ . This spectrum-to-spectrum error estimate  $\sigma(s-s)$  is given in column 5 of Table 1. We then compared this to the overall standard deviation of the velocities  $\sigma$  (column 6 of Table 1), and set the criterion for variability as  $\sigma/\sigma(s-s) > 3.3$ , which corresponds to the  $< 1\%$  probability that both variances are drawn from the same population (for 9 degrees of freedom = 10 observations minus 1 mean value). We found that three of the ten single-lined targets were velocity variable according to this criterion (see the final column of Table 1). The stars HD 17520 and BD+60°594 are probably long period binary systems while the very luminous star HD 15570 exhibits variations related to atmospheric structure fluctuations (see the discussion in §6).

The spectra of the targets DN Cas and BD+60°497 both showed evidence of line-doubling in some observations, and the spectra of HD 17505A displayed three components in the best separated cases. We were able to use a tomography algorithm to isolate the stationary line component in HD 17505A (§6.5), and after removal of the stationary component the spectra were treated in the same way as for the other double-lined systems. We measured velocities for these double-lined binaries in a two-step process (Gies et al. 2002). Preliminary radial velocities were found using the multiple Gaussian fitting technique within the IRAF SPLOT routine. Then preliminary orbital elements were determined that provided starting estimates of the velocities for both components in each spectrum. We then formed template spectra for both components by interpolating in the O-star synthetic spectrum grid of Lanz & Hubeny (2003) for a temperature and gravity appropriate for each star, and these were convolved with broadening functions to account for rotational and instrumental broadening (§4). Then we obtained velocities for specific spectral lines by a non-linear least squares fit

of the observed profile with the two template spectra profiles co-added with a pre-defined monochromatic flux ratio (details are given for each case in §6). We took care to form an average velocity for each spectrum based on the same set of selected lines in order to avoid spurious variations introduced by line-to-line velocity differences. The resulting velocities are given below in §6 (Tables 4, 6, and 8).

We determined orbital elements for these three double-lined binaries using the non-linear, least-squares fitting routine of Morbey & Brosterhus (1974). The starting value for the orbital period was obtained with the period search technique of Scargle (1982) as modified by Horne & Baliunas (1986) (or from photometry in the case of DN Cas). We first solved for the best fit period and then we formed separate elliptical solutions for both the primary and secondary components. The derived eccentricity in the case of DN Cas was not significantly different from zero (Lucy & Sweeney 1971), but in the other two targets the eccentricity was significant and the same within errors in the solutions for the primary and secondary components. We formed average values of the eccentricity  $e$ , longitude of periastron  $\omega$ , and time of periastron  $T$  that were then fixed in solutions to obtain the semiamplitude  $K$  and systemic velocity  $\gamma$  for the primary and secondary components individually (since differing atmospheric expansion rates may lead to different systemic velocities). The final orbital elements are given in §6 (Tables 5, 7, and 9).

#### 4. Stellar Parameters

We co-added our spectra to form high S/N versions for use in spectral classification, temperature and gravity estimation, and measurement of the projected rotational velocity  $V \sin i$ . We used a simple shift-and-add algorithm to form an average spectrum in the case of the single-lined targets. However, we relied upon the Doppler tomography algorithm described by Bagnuolo et al. (1994) to reconstruct the individual component spectra of the multiple component systems. The tomography algorithm is an iterative scheme that uses the derived orbital velocity shifts and monochromatic flux ratio to estimate the spectra of each component. We ran the algorithm for 50 iterations with a gain of 0.9, although the results are insensitive to both parameters. The final, continuum rectified spectra of all our targets (except HD 17505; see §6.5) and all their components are shown in Figures 1 and 2 in order of decreasing effective temperature.

We estimated the spectral classification of each target (Table 1) by comparing their spectra with standard star spectra in the atlas of Walborn & Fitzpatrick (1990). The corresponding stellar effective temperature  $T_{\text{eff}}$  was determined by comparing the equivalent widths of various He II/He I line ratios with those measured in the synthetic spectral library

for O-stars by Lanz & Hubeny (2003). In most cases, we simply assumed a surface gravity of  $\log g = 4.0$  as a suitable value for main sequence stars, but this approach was inadequate in several cases of evolved stars where the H Balmer line wings are narrower and indicative of a lower gravity. We experimented with a number of model synthetic spectra to best estimate the gravity in these cases. This was accomplished through comparing models by eye with the data in order to find an appropriate match for surface gravity. The most difficult spectrum to match was that of the very luminous star HD 15570, which displays clear evidence of the atmospheric expansion into a stellar wind that is not included in the static atmosphere formulation adopted by Lanz & Hubeny (2003). We estimate that our fitting errors are approximately  $\pm 1000$  K in temperature and  $\pm 0.3$  dex in  $\log g$ , and the results are listed in Table 1.

We estimated the projected rotational velocity  $V \sin i$  by comparing the observed He I and He II line widths with those found by convolving the model profiles from Lanz & Hubeny (2003) with instrumental and rotational broadening functions. The instrumental broadening of our spectra was represented by a Gaussian with  $\text{FWHM} = 52 \text{ km s}^{-1}$ . The rotational broadening function (Gray 1992) was computed assuming a spherical star with a linear limb-darkening coefficient determined from Wade & Rucinski (1985). A grid of theoretical profiles was computed for a range of  $V \sin i$ , and a  $\chi^2$  minimization was used to determine the best fit to the data. The results and errors are listed in Table 1. Note that this approach does not account for variations in the intensity profile across the disk, nor the non-spherical shape and gravity darkening found in rapid rotators (Townsend, Owocki, & Howarth 2004). These shortcomings are most important for the two rapid rotators in our sample, BD+60°513 and BD+60°594, and we have probably underestimated the true rotational broadening in these cases.

## 5. Radii from Fits of the Spectral Energy Distributions

All of our targets are considered to be members of the Cas OB6 association based upon their position in the sky and placement in the Hertzsprung-Russell diagram (HRD) (Voroshilov et al. 1985; Garmany & Stencel 1992; Walborn 2002). The proper motion study of IC 1805 made by Vasilevskis, Sanders, & van Altena (1965) confirms membership for five targets but curiously indicates a somewhat discrepant proper motion for HD 15558. We will assume that all the targets share a common distance, so their observed fluxes are directly related to their relative stellar radii. Since we have determined temperature and multiplicity for each target, we have all parameters needed to estimate their radii as a function of distance by comparing their observed and model flux distributions, and we can then check the distance

by comparing the derived and model radii (as a function of temperature). The angular diameter of the limb darkened disk  $\theta_{LD}$  (in units of radians) is found by the inverse-square law:

$$\frac{f_{\lambda}(\text{observed})}{F_{\lambda}(\text{emitted}) 10^{-0.4A_{\lambda}}} = (R_{\star}/d)^2 = \frac{1}{4}\theta_{LD}^2 \quad (1)$$

where the ratio of the observed and emitted fluxes (reduced by the effects of interstellar extinction  $A_{\lambda}$ ) depends on the square of the ratio of stellar radius  $R_{\star}$  to distance  $d$ . All our targets have a large reddening, so we need to fit the relation above over the entire observed spectrum in order to account reliably for the wavelength dependent shape of the extinction curve. We adopted the extinction curve law from Fitzpatrick (1999) that is a function of the reddening  $E(B - V)$  and the ratio of total-to-selective extinction  $R = A_V/E(B - V)$ . We then fit the observed flux distribution of each target to determine  $E(B - V)$ ,  $R$ , and angular diameter  $\theta_{LD}$ .

We compiled data on the observed fluxes from the UV to the near-IR. There are low dispersion *International Ultraviolet Explorer (IUE)* spectra available (SWP and LWR cameras) for all of the targets except DN Cas, HD 17520, HD 237019, and BD+60°586, and we formed binned versions of the UV spectral fluxes from these. We found Johnson *UBV* photometry for all the targets (plus Cousins *RI* in a few cases), and these magnitudes were transformed to fluxes using the calibration of Colina, Bohlin, & Castelli (1996). We also included Strömberg photometry for 7 of the 13 targets using the calibration of Gray (1998). All of the stars are included in the *2MASS All-Sky Catalog of Point Sources* (Cutri et al. 2003), and we converted the *JHK* magnitudes to fluxes using the calibration of Cohen, Wheaton, & Megeath (2003).

The model fluxes were selected from the grid of Lanz & Hubeny (2003) based upon the values of  $T_{\text{eff}}$  and  $\log g$  in Table 1. These model fluxes are based upon plane-parallel, non-LTE, line blanketed atmospheres that do not include the effects of stellar wind mass loss. However, the inclusion of winds generally alters the spectral energy distributions only at wavelengths much larger and much smaller than those considered here (Martins, Schaerer, & Hillier 2005), so wind effects are insignificant in this context. We co-added model fluxes using the observed flux ratios for the spectroscopic binaries and using the observed magnitude difference for close visual binaries (details are given in next section for individual stars). Note that in the two single-lined binary cases, HD 17520 and BD+60°594, we simply assumed that the unseen companion contributes 5% of the total flux (a compromise between the expectation that the mass ratio is not too extreme and that brighter companions would have visible spectral features in our observations). We have no spectral information for some of the companions, and in these cases we assumed that the companion was a main sequence star with a temperature corresponding to the observed flux ratio (from the calibration in

Table 4 of Martins et al. 2005). We set a lower limit of  $T_{\text{eff}} = 27500$  K and  $\log g = 4.0$  for the faint companions, which corresponds to the cool boundary in the grid of Lanz & Hubeny (2003). This simplification is acceptable since any detected companion is probably hot enough that the optical and near-IR regions correspond to the common Rayleigh-Jeans portion of the flux distribution.

We compared the observed and model flux distributions and made a grid search fit to find the values of  $E(B - V)$  and  $R$  that produced the lowest  $\chi^2_{\nu}$  residuals (by weighting the observations approximately equally between the UV, optical, and near-IR bands). The normalization term in the final fit yields the angular diameter. Our results are gathered in Table 3 which lists the star name, home cluster, angular diameter (in micro-arcsec), derived radius (see below),  $E(B - V)$ , and  $R$ . The accompanying error estimates for  $E(B - V)$  and  $R$  are derived from the point in grid search where  $\chi^2_{\nu}$  attains a value higher by 1 than normalized minimum value, and the errors in diameter are based upon the scatter in flux distribution fit and the errors propagated from uncertainty in  $T_{\text{eff}}$ ,  $E(B - V)$ , and  $R$ . The model fits were generally excellent, but they were less satisfactory for the spectra of the three hottest stars, where it was difficult to find a consistent match of the far- and near-UV fluxes. We also found the  $JHK$  fluxes were too large relative to the optical fluxes for HD 17520, which we suspect is due to an IR excess associated with the Be disk emission of the companion (Porter & Rivinius 2003), so the fit was based on the optical fluxes alone in this case.

The stellar radius is found by

$$R_{\star} = 107.43 R_{\odot} \theta_{LD} d \tag{2}$$

where the distance  $d$  is given in kpc. The distance estimates for IC 1805 and IC 1848 range from 1.9 kpc (Ishida 1970) to 2.4 kpc (Guetter & Vrba 1989) (with a scatter of  $\pm 10\%$  among recent estimates). We selected a distance of  $d = 1.886$  kpc from the compendium of open cluster data by Loktin et al. (2001) because this low end value appears to give the best match between the observed and theoretical stellar radii and provides good agreement with radii of similar stars in eclipsing binaries (Gies 2003). The resulting radii are listed in Table 3 and are plotted against stellar temperature in Figure 3. There is a clear and consistent trend for the hotter main sequence stars to be larger, and the observations match the predictions for main sequence stars from the atmosphere models of Martins et al. (2005) (shown as a dotted line in Fig. 3). We also show in Figure 3 the  $(T_{\text{eff}}, R_{\star})$  loci for stars with ages of 1.00 and 3.16 Myr from the evolutionary models of Lejeune & Schaerer (2001), which correspond to the age range for IC 1805 given by Massey et al. (1995). We see that most of the stars fall within the expected region in this diagram for this age range. However, the positions of several stars indicate that there is a real dispersion in the ages among this sample. For

example, BD+60°501 appears to have a relatively small radius for its temperature, indicating it is the youngest object in our sample. The derived stellar radii are directly proportional to the assumed distance, and, for example, if we adopted the larger distance  $d = 2.34$  kpc advocated by Massey et al. (1995) then the stars would be approximately 24% larger, a size that would be difficult to reconcile with the evolutionary models of Lejeune & Schaerer (2001). We show below that our derived radii for DN Cas agree well with those determined independently from an analysis of the eclipsing light curve.

## 6. Results for Individual Objects

### 6.1. Stars With Constant Radial Velocity

BD+60°501.– The two Balmer lines  $H\gamma$  and  $H\beta$  have the lowest measured velocities in the template spectrum, so they were omitted from the average (i.e., based only on the He I and He II lines). Our observed mean velocity of  $-57.9 \pm 1.1$  km s<sup>-1</sup> is reasonably consistent with the mean from the work of Rauw & De Becker (2004) of  $-49.9 \pm 2.5$  km s<sup>-1</sup> who also find the star to be a constant velocity object.

HD 15558.– There is evidence here for a velocity progression (lower velocity among low excitation lines), so we used only the lines He II  $\lambda\lambda 4199, 4541$  to set the radial velocity of the template spectrum. There are no obvious variations over the 5 night run, but the star may be a long period, single-lined binary (Garmany & Massey 1981). According to the recent orbital elements from Stickland & Lloyd (2001), the orbital period is  $439.64 \pm 0.26$  d and the predicted velocity at the mean time of our observations is  $-21.8$  km s<sup>-1</sup> (near the peak of the radial velocity curve), which is  $27.7$  km s<sup>-1</sup> higher than our observed mean of  $-49.5 \pm 2.9$  km s<sup>-1</sup>. This discrepancy could be caused by differences in measurement techniques or errors in the preliminary orbital solution of Stickland & Lloyd (2001). A long-term study by M. De Becker and G. Rauw (2005, private communication) has recently confirmed the binary status of this star and will provide an improved orbital solution. Therefore, we list this star as “constant (SB1)” in Table 1 denoting both a lack of short term line variability in our observations as well as the recent confirmation of binarity. There is a visual companion at a separation of 9''9 that is 2.6 mag fainter (Perryman 1997).

HD 15570.– There is a clear velocity progression between spectral lines with the low excitation lines (H, He I) appearing at a much lower velocity than the high excitation lines (He II, N V). There is also a correlation with line width in the sense that stronger, broader lines have lower velocity. We adopted a radial velocity for the template spectrum from the lines He II  $\lambda\lambda 4199$  and N V  $\lambda\lambda 4604, 4620$ . The night-to-night scatter between velocities is

small except on the last night when the measured velocity is  $\approx 10 \text{ km s}^{-1}$  more positive than the mean from the other nights. Curiously, the Of emission lines do not show any shift in velocity on the final night. We suspect that the change was related to an atmospheric fluctuation rather than orbital motion. Underhill & Gilroy (1990) also consider this star to be a velocity variable. De Becker, Rauw, & Eenens (2005) find no evidence of orbital motion and discuss rotational modulation as a possible source of line variability.

HD 15629.– The low excitation Balmer and He I lines have systematically low velocities, so the template mean was adopted from the lines He II  $\lambda\lambda 4199, 4541, 4686$ . We find no evidence of velocity variability. Underhill & Gilroy (1990), on the other hand, flag this star as possibly variable, but given the presence of line-to-line velocity differences, some of the velocity differences found by various authors are probably due to the line sample adopted (and not to orbital motion). De Becker et al. (2005) also find no evidence of orbital motion for this star.

BD+60°513.– This star has a broad-lined spectrum, and we selected only the strongest lines to measure the template mean velocity ( $\text{H}\gamma$ ,  $\text{H}\beta$ , He I  $\lambda\lambda 4471, 4921$ , He II  $\lambda\lambda 4541, 4686$ ). We confirm the lack of short term velocity variability reported by Rauw & De Becker (2004), and our mean velocity of  $-58.6 \pm 2.8 \text{ km s}^{-1}$  is probably consistent with their mean value,  $-44.3 \pm 10.5 \text{ km s}^{-1}$ .

BD+62°424.– The  $\text{H}\beta$  line had the lowest velocity measured, so we omitted the H Balmer lines and weak lines in forming the template mean velocity. The star appears to be radial velocity constant over the run, and our mean velocity,  $-34.3 \pm 1.7 \text{ km s}^{-1}$ , is probably consistent with that from Abt et al. (1972) of  $-43.5 \pm 6.3 \text{ km s}^{-1}$ .

HD 237019.– All the strong lines were used to form the template mean velocity. The star has a constant radial velocity over the run. Our mean velocity of  $-43.4 \pm 1.1 \text{ km s}^{-1}$  is higher than the only other value in the literature of  $-68 \text{ km s}^{-1}$  from Seyfert & Popper (1941).

BD+60°586.– We omitted  $\text{H}\beta$  and He I  $\lambda 4921$  from the template mean calculation, since both lines had significantly lower velocities. The star was radial velocity constant during the run. Our mean velocity,  $-48.1 \pm 1.0 \text{ km s}^{-1}$ , agrees with that found by Abt et al. (1972),  $-42.3 \pm 7.1 \text{ km s}^{-1}$ , but is lower than the value reported by Conti et al. (1977),  $-27.9 \pm 1.2 \text{ km s}^{-1}$ . The star is a member of a visual multiple system (ADS 2194) with companions at separations of  $7''.2$  ( $\Delta V = 1.7$ ) and  $13''.0$  ( $\Delta V = 4.7$ ).

## 6.2. Single-lined Spectroscopic Binaries

HD 17520.– The  $H\beta$  line has a blue-shifted emission component which also appears weakly in  $H\gamma$ . The Balmer lines and weak lines were omitted in the calculation of the template mean velocity. The velocities show a progressive increase over the duration of the run, reaching values similar to those observed by Conti et al. (1977) and Liu et al. (1989). Walter (1992) showed how  $H\alpha$  emission developed between 1985 and 1991 leading to a spectral classification as a Be-type star (probably its status in 2003 as well since the emission is so apparent in  $H\beta$ ). This star is also the central object in a visual multiple system (ADS 2165) with a close companion at a separation of  $0''.335$  and with a magnitude difference of 0.52 mag (Perryman 1997; Walborn 2002). Our spectra show evidence of only one set of lines (for the O9 V component), and unfortunately, we do not know if the Be emission originates in the O-star or its nearby companion (which could have broad shallow lines as observed in many Be stars). We note that over the course of the run the  $H\beta$  emission appeared to be almost stationary while the absorption lines shifted red-ward by  $\approx 17 \text{ km s}^{-1}$ . The simplest interpretation is that the O-star component is a long-period, single-lined binary, while the Be emission originates in the fainter component of the close visual pair. There is another star at a separation of  $10''.8$  that is 3.2 mag fainter in  $K$  (Cutri et al. 2003).

BD+60°594.– We used the strong lines to set the template mean velocity for the broad-lined spectrum of this star. The first measured velocity is close to the value obtained by Conti et al. (1977),  $-50.5 \pm 5.6 \text{ km s}^{-1}$ , but the subsequent velocities decline monotonically by  $\approx 49 \text{ km s}^{-1}$  over the next 4 days. This suggests that the star is a single-lined binary with a period of  $\approx 20 \text{ d}$  and a semiamplitude of  $\approx 50 \text{ km s}^{-1}$ .

## 6.3. The Double-Lined Eclipsing System DN Cas

DN Cas has been known as an eclipsing binary for some time and was classified as an Algol type binary with a period of 1.155479 d by Hoffmeister (1947). Hiltner (1956) classified the spectrum as O8 V. A later photometric study by Frazier & Hall (1974) used  $UBV$  photoelectric photometry to refine the orbital period to 2.310955 d, twice that of the original value. Unfortunately, the comparison star used by Frazier & Hall (1974) turned out to be itself an eclipsing binary, compromising their final photometry. Davidge (1980) made another photometric study, and based upon the curvature near the maxima of the light curve he reclassified DN Cas as a  $\beta$  Lyrae type system. Interestingly no spectroscopic observations of DN Cas have appeared in the literature, though Davidge (1980) claimed that such observations were underway. Additionally, the only photometry that has been published, other than in phase-folded figures, is the compromised data of Frazier & Hall

(1974). This overlooked opportunity to obtain masses for this massive binary is rectified here, where we present the first full orbital solution based on our spectroscopy and photometry from the literature.

We determined velocities for both components using non-linear least-squares fits of two templates with temperatures and rotational velocities given in Table 1 and with a monochromatic flux ratio in the blue of  $F_2/F_1 = 0.41 \pm 0.10$ . Our final radial velocities are given in Table 4 and the spectroscopic orbital elements are given in Table 5. The period was adopted from the eclipse timing observations collected by Kreiner, Kim, & Nha (2001). Here we adopt the time of minimum light (primary superior conjunction) to set the zero-point of orbital phase and epoch  $T_{\min}$ , and our derived epoch agrees with the current photometric epoch of minimum light from Kreiner et al. (2001) of HJD 2,452,501.928  $\pm$  0.007. Eccentric fits offered no significant improvement over circular fits (Lucy & Sweeney 1971), so circular elements are given in Table 5. The radial velocities and orbital solutions are shown in Figure 4.

The only published photometric data of DN Cas are those from Frazier & Hall (1974) who made *UBV* photoelectric observations between 1971 October and 1972 December. Unfortunately, their comparison star, HD 14817, is itself an eclipsing binary as mentioned above. However, the light curve of HD 14817 from *Hipparcos* (Perryman 1997) is flat outside of eclipse, so we can retain the results from Frazier & Hall (1974) that are based on outside-of-eclipse times for HD 14817. These measurements are plotted against orbital phase in Figure 5, and because there remain significant phase gaps in this restricted set, our light curve fitting results should be considered preliminary.

We calculated a model light curve using the Wilson-Devinney code (Wilson & Devinney 1971; Wilson 1990). Most of the model parameters are set by the spectroscopic orbital solution (Table 5), the adopted temperatures and gravities from the spectra (Table 1), the associated limb darkening parameters (Van Hamme 1993), and the monochromatic flux ratio (which sets the ratio of the mean stellar radii). In addition, we set the bolometric albedo and gravity darkening exponents to 1.0, which are valid approximations for stars with fully radiative envelopes. We then fit the observed *V*-band observations by varying the inclination  $i$  and the stellar radii. The ratio of stellar radii was set using the observed monochromatic flux ratio and model surface flux ratio (set according to the temperatures and gravities in Table 1)

$$R_2/R_1 = [(f_\lambda(\text{observed})_2/f_\lambda(\text{observed})_1) \times (F_\lambda(\text{emitted})_1/F_\lambda(\text{emitted})_2)]^{0.5} = 0.72 \pm 0.09.$$

If the stars are rotating synchronously, then the ratio of projected rotational velocities also yields the ratio of radii as

$$R_2/R_1 = (V \sin i)_2/(V \sin i)_1 = 0.72 \pm 0.15$$

and the good agreement between these two estimates suggests that synchronous rotation has been attained in this close binary. We found that the radii obtained from a fit of the spectral energy distribution and distance of 1.9 kpc (Table 3) led to an excellent fit of the light curve for an orbital inclination of  $i = 79.2 \pm 1.1$  (Fig. 5), and the derived stellar masses are  $M_1 = 19.2 \pm 0.8 M_\odot$  for the O8 V primary and  $M_2 = 13.9 \pm 0.5 M_\odot$  for the B0.2 V secondary (Table 5). The mass of the primary is consistent with its spectral type for the calibration given by Martins et al. (2005), and the mass of the secondary agrees well with the mass for its spectral type according to the relations given by Hanson, Howarth, & Conti (1997). Both stars are well within their respective Roche lobes.

There is a companion to DN Cas in the 2MASS catalogue at a separation of  $5''.3$  and at a position angle of  $89^\circ$ . However, inspection of the 2MASS images at this position suggests that this object is probably not a real star since its point spread function looks very sharp and unlike those of nearby stars. Furthermore, we see no evidence of such a tertiary in our observations. Since the near east-west alignment of the putative object and DN Cas is the same as the slit orientation for our KPNO 4 m spectra, the tertiary should appear in our spectra with a separation from DN Cas of 7.7 pixels in the spatial dimension. The average 2MASS magnitude difference is 2.13 mag (for  $H, K$ ), so that the flux ratio of tertiary to binary is 0.14 in the near-IR. However, our blue spectra show no sign of a companion brighter than  $\Delta m = 5$ , so if this companion is real, it is probably a very red foreground star that can be ignored in our analysis. We found that the introduction of a third light contribution of 14% in the  $V$ -band light curve results in an increase in the inclination by  $3^\circ$ , but since the actual flux contribution of a tertiary is probably much smaller than this, any changes in our results due to the presence of a tertiary are probably comparable to or less than the errors quoted in Table 5.

#### 6.4. The Double-Lined System BD+60°497

The spectra of BD+60°497 show clear evidence that this star is a double-lined spectroscopic binary. In their recent paper, Rauw & De Becker (2004) give the first orbital solution for BD+60°497, and they find an orbital period of 3.96 days. We measured velocities using the scheme outlined in §3 by matching template synthetic profiles for models with temperatures and gravities given in Table 1, together with an estimated flux ratio of  $F_2/F_1 = 0.35 \pm 0.08$ . We note, however, that in some of the lines (for example, He I  $\lambda\lambda 4387, 4471$ ) we found that the approaching, blue-shifted component (primary and secondary) often appeared to be weaker than expected based upon this fixed flux ratio (Rauw & De Becker 2004 also observed a similar variation). We doubt that this variation has a

significant effect on our measurements, which appear in Table 6.

We combined our velocities with those of Rauw & De Becker (2004) in making the orbital solution. A number of alias periods remain viable, but we obtained the best fit with a period close to that obtained by Rauw & De Becker (2004) (see Table 7). However, unlike Rauw & De Becker (2004), we found that a significant eccentricity is present, and we made full elliptical fits for both components. Otherwise our results are in reasonable agreement with their solution (compared in Table 7). The velocities and orbital fit are shown folded on the derived ephemeris in Figure 6. Assuming masses typical of their spectral classes (Martins et al. 2005), the system probably has an inclination of  $i \approx 47^\circ$ , so we do not expect eclipses to occur.

### 6.5. The Multiple Star System HD 17505

The star system HD 17505 dominates the center of the cluster IC 1848, and there are seven visual companions noted by Mason et al. (1998) at distances ranging from  $2''.1$  to  $124''.0$ . Multiplicity in the central object HD 17505A has been discussed by Conti & Alschuler (1971), Walborn (1973), Howarth et al. (1997), and Walborn (2002) and it is known to contain at least three stars since the single *International Ultraviolet Explorer* spectrum shows evidence of three Doppler shifted components (Stickland & Lloyd 2001). Walborn (2002) pointed out that the multiplicity of the star is the reason it appears so bright in the HRD. We obtained 10 spectra of HD 17505A over the five night duration of the KPNO 4 m run, and we found that the lines were strongly blended in all but a few spectra corresponding to the maximum Doppler separation of the binary motion. However, we also obtained an additional 32 red spectra of the target in 2000 with the KPNO 0.9 m Coude Feed telescope (§3), and these turned out to be particularly helpful in finding the orbital elements.

Initial inspection of these higher dispersion red spectra showed that all three components were cleanly resolved in the He I profiles observed near orbital quadrature phases and indicated an orbital period of approximately 8 days. We measured radial velocities by first making unconstrained three-Gaussian fits of the least blended feature, He I  $\lambda 7065$ , in the quadrature phase spectra. We obtained a preliminary orbital solution from this subset of spectra for the two moving components, and then we used this solution to estimate the Doppler shifts for all the Coude Feed observations. Then we made three-component Gaussian fits of He I  $\lambda 7065$  in all the red spectra using these starting estimates for the Doppler shifts and constraining the widths to be the mean values found from the fits of the quadrature phase spectra. A new orbital solution was obtained, and the solution was used to make a three component reconstruction of the individual component spectra using the Doppler

tomography algorithm (Bagnuolo et al. 1994). We subtracted the reconstructed spectrum of the stationary component from each spectrum and renormalized them to end up with a set corresponding to the spectra of the double-lined binary alone. We then measured the radial velocities using the non-linear, least-squares method by matching template spectra to the profiles of  $H\alpha$ , He I  $\lambda 6678$ /He II  $\lambda 6683$ , and He I  $\lambda 7065$ . The template spectra for the two components were taken from their respective tomographic reconstructions ( $F_2/F_1 = 1.0 \pm 0.1$ ) rather than using the model profiles from Lanz & Hubeny (2003), because we were concerned that some of these red features are not well represented by the synthetic models. This approach worked well except in one conjunction phase observation (from HJD 2,451,892.743) where the lines were too badly blended for reliable measurement. Our final radial velocities from the red spectra for the close binary are collected in Table 8.

The estimate for the orbital period from the red spectra alone was  $P = 8.572 \pm 0.003$  d, and the error was sufficiently small that we could determine the cycle number and approximate orbital phase corresponding to the times of the KPNO 4 m observations in 2003 October. We measured the line width of the He I  $\lambda 4471$  feature in these blue spectra to find that maximum velocity separation occurred at HJD 2,452,915.469  $\pm 0.12$ , and we compared this to the time of the same orbital phase for the 2000 Coude Feed observations to arrive at a revised period estimate of  $P = 8.5710 \pm 0.0008$  d. The final orbital solution is given in Table 9 and the radial velocity curve appears in Figure 7. The predictions from this fit for the time of the *IUE* observation are +128 and  $-184$  km s $^{-1}$ , in reasonable agreement with the observed velocities of +142 and  $-165$  km s $^{-1}$  (Stickland & Lloyd 2001), but we did not include the *IUE* measurements in the final solutions because of possible systematic differences between velocities measured in the UV and optical.

We made tomographic reconstructions of both the blue and red spectra using the orbital solution in Table 9 and assuming flux contributions of 30%, 30%, and 40% for Aa1, Aa2, and Ab, respectively (based upon the relative equivalent widths of the He I  $\lambda 6678$  + He II  $\lambda 6683$  feature). Both the blue and red spectral reconstructions are plotted in Figure 8. We determined radial velocities of the stationary component Ab of  $-30 \pm 3$  and  $-38 \pm 5$  from the blue and red reconstructed spectra, respectively. Once again, the optical velocities are systematically more negative than the UV determined value for Ab of  $-13.5$  km s $^{-1}$  (Stickland & Lloyd 2001). Our results are summarized in a schematic representation of the system hierarchy in Figure 9. Note that the Coude Feed spectra were made with a  $2''.5$  wide slit in an approximately north-south orientation, so the B component (at a separation of  $2''.15$  and a position angle of  $93^\circ$  with a magnitude difference of  $\Delta H_p = 1.66$  mag; Perryman 1997) may be slightly mixed in with the light from the Ab component for the red reconstructed spectrum. However, the 4 m spectra were made with an east-west slit orientation, so it was possible to separate the A and B components spatially along the slit. A single

extracted spectrum of the B component is shown in Figure 8 along with the tomographic reconstructions of the Aa1, Aa2, and Ab components. The spectrum of the B component is clearly different and indicates a cooler effective temperature than the stars of component A, and, thus, the spectroscopic triple we detect is clearly related to A alone. The hottest and brightest of all the components is Ab, and its spectral type agrees with that obtained by Walborn (1972) for the entire system.

The stars of the Aa1-Aa2 central binary are far enough apart that no eclipses should be seen, and indeed none are observed (Perryman 1997). For example, if we adopt the masses and radii associated with O-type main sequence stars from Martins et al. (2005), then the expected system inclination should be  $i = 65^\circ$  (based upon the  $M \sin^3 i$  values in Table 9) while eclipses would be observed only if  $i > 73^\circ$  (based upon the semimajor axis in Table 9). The orbital period of B around the triple A can be estimated as  $\approx 27,000$  y if we take the projected angular separation as the semimajor axis and the distance is 1.9 kpc. The orbital period of the Aa-Ab central triple is probably much less. The system was unresolved in the speckle survey of Mason et al. (1998), and if we take their resolution limit of 35 mas as the projected semimajor axis then the orbital period should be  $< 61$  y. The target is clearly worthy of continued spectroscopic and interferometric observation to search for evidence of such orbital motion.

## 7. Summary

We have monitored thirteen O stars in the Cas OB6 association in search of multiple star systems. Five of the thirteen were found to have radial velocity variations related to orbital motion. Of these five, we have determined orbital solutions for three double-lined systems: the eclipsing binary DN Cas, BD+60°497, and the spectroscopic triple HD 17505A. The remaining two binaries, BD+60°594 and HD 17520, are single-lined binaries with periods longer than 5 days. In addition to these five, one of our targets, HD 15558, is probably a long period binary (Garmany & Massey 1981; Stickland & Lloyd 2001). One other bright O-star in Cas OB6 is HD 16429, which was found by McSwain (2003) to be a spectroscopic triple. If we include all of these objects in the known sample of observed O-stars in the Cas OB6 association, then we find that 7 of the 14, or 50%, are spectroscopic binaries. This value is well within the range found by Mason et al. (1998) for spectroscopic binaries among stars in clusters and associations.

We note that two systems, HD 17505 and DN Cas, are of special interest and would benefit from follow-up observations. We are planning to obtain new three-color photometry of the eclipsing binary DN Cas in order to make a better fit of the light curve and to determine

an accurate mass of the O8 V primary star. The multiple system HD 17505 is a fascinating system with at least four O stars (with a total mass close to  $100 M_{\odot}$ ) which are apparently gravitationally bound. High resolution studies via interferometry to separate the Aa and Ab components would produce a more accurate kinematic model for the system and would help us better understand stellar interactions in these systems and their role in the formation and ejection of massive stars.

We are grateful to the director and staff of KPNO for their help in making these observations possible. We also thank Gregor Rauw and Michael De Becker for sharing their results with us in advance of publication. Financial support was provided by the National Science Foundation through grant AST–0205297 (DRG). Institutional support has been provided from the GSU College of Arts and Sciences and from the Research Program Enhancement fund of the Board of Regents of the University System of Georgia, administered through the GSU Office of the Vice President for Research. MVM is supported by an NSF Astronomy and Astrophysics Postdoctoral Fellowship under award AST–0401460. This publication makes use of data products from the Two Micron All Sky Survey, which is a joint project of the University of Massachusetts and the Infrared Processing and Analysis Center/California Institute of Technology, funded by the National Aeronautics and Space Administration and the National Science Foundation. This research has also made use of the Washington Double Star Catalog maintained at the U.S. Naval Observatory.

## REFERENCES

- Abt, H. A., Levy, S. G., & Gandet, L. 1972, *AJ*, 77, 138
- Bagnuolo, W. G. Jr., Gies, D. R., Hahula, M. E., Wiemker, R., & Wiggs, M. S. 1994, *ApJ*, 423, 446
- Bohannon, B., & Garmany, C. D. 1978, *ApJ*, 223, 908
- Bolton, C. T., & Rogers, G. L. 1978, *ApJ*, 222, 234
- Boyajian, T. S., et al. 2005, *ApJ*, 621, 978
- Carpenter, J. M., Heyer, M. H., & Snell, R. L. 2000, *ApJS*, 130, 381
- Cohen, M., Wheaton, W. A., & Megeath, S. T. 2003, *AJ*, 126, 1090
- Colina, L., Bohlin, R., & Castelli, F. 1996, HST Instrument Science Report CAL/SCS-008 (Baltimore: STScI)

- Conti, P. S., & Alschuler, W. R. 1971, *ApJ*, 170, 325
- Conti, P. S., Leep, E. M., & Lorre J. J. 1977, *ApJ*, 214, 759
- Cutri, R. M., et al. 2003, *The 2MASS All-Sky Catalog of Point Sources* (Pasadena: IPAC/Cal. Inst. Tech.)
- Davidge, T. J. 1980, *IBVS*, 1817
- De Becker, M., Rauw, G., & Eenens, P. 2005, *MNRAS*, submitted
- Fitzpatrick, E. L. 1999, *PASP*, 111, 63
- Foster, T., & Routledge, D. 2003, *ApJ*, 598, 1005
- Frazier, T. H., & Hall, D. S. 1974, *PASP*, 86, 661
- Garcia, B., & Mermilliod, J. C. 2001, *A&A*, 368, 122
- Garmany, C. D., Conti, P. S., & Massey, P. 1980, *ApJ*, 242, 1063
- Garmany, C. D., & Massey, P. 1981, *PASP*, 93, 500
- Garmany, C. D., & Stencel, R. E. 1992, *A&AS*, 94, 211
- Gies, D. R. 2003, in *A Massive Star Odyssey, from Main Sequence to Supernova*, IAU Symposium No. 212 (ASP Conf. Ser. Vol.), ed. K. A. van der Hucht, A. Herrero, & C. Esteban (San Francisco: ASP), 91
- Gies, D. R., Penny, L. R., Mayer, P., Drechsel, H., & Lorenz, R. 2002, *ApJ*, 574, 957
- Gies, D. R., & Bolton, C. T. 1986, *ApJS*, 61, 419
- Gray, D. F. 1992, *The Observation and Analysis of Stellar Photospheres*, 2nd ed. (Cambridge: Cambridge Univ. Press)
- Gray, R. O. 1998, *AJ*, 116, 482
- Guetter, H. H., & Vrba, F. J. 1989, *AJ*, 98, 611
- Hanson, M. M., Howarth, I. D., & Conti, P. S. 1997, *ApJ*, 489, 698
- Hayford, P. 1932, *Lick Obs. Bull.*, 16, 53
- Hiltner, W. A. 1956, *ApJS*, 2, 389

- Hoffmeister, C. 1947, Veroff. Sternw. Sonneberg, 1, 81
- Hoogerwerf, R., de Bruijne, J. H. J., & de Zeeuw, P. T. 2001, A&A, 365, 49
- Horne, J. H., & Baliunas, S. L. 1986, ApJ, 302, 757
- Howarth, I. D., Siebert, K. W., Hussain, G. A. J., & Prinja, R. K. 1997, MNRAS, 284, 265
- Hutchings, J. B. 1976, ApJ, 203, 438
- Ishida, K. 1970, PASJ, 22, 277
- Kreiner, J. M., Kim, C., & Nha, I. 2001, An Atlas of  $O - C$  Diagrams of Eclipsing Binary Stars (Cracow: Wydawnictwo Naukowe Akad. Pedagogicznej)
- Lanz, T., & Hubeny, I. 2003, ApJS, 146 417
- Lejeune, T., & Schaerer, D. 2001, A&A, 366, 538
- Levato, H., Malaroda, S., Morell, N., Garcia, B., & Hernandez, C. 1991, ApJS, 75, 869
- Liu, T., Janes, K. A., & Bania, T. M. 1989, AJ, 98, 626
- Liu, T., Janes, K. A., & Bania, T. M. 1991, AJ, 102, 1103
- Loktin, A. V., Gerasimenko, T. P., & Malysheva, L. K. 2001, Astron. Astrophys. Trans., 20, 607
- Lucy, L. B., & Sweeney, M. A. 1971, AJ, 76, 544
- Martins, F., Schaerer, D., & Hillier, D. J. 2005, A&A, 436, 1039
- Mason, B. D., Gies, D. R., Hartkopf, W. I., Bagnuolo, W. G., ten Brummelaar, T., & McAlister, H. A. 1998, ApJ, 115, 821
- Massey, P., Johnson, K. E., & DeGioia-Eastwood, K. 1995, ApJ, 454, 151
- McSwain, M. V. 2003, ApJ, 595, 1124
- Morbey, C. L., & Brosterhus, E. B. 1974, PASP, 86 455
- Normandeau, M., Taylor, A. R., & Dewdney, P. E. 1996, Nature, 380, 687
- Perryman, M. A. C. 1997, The Hipparcos and Tycho Catalogues, ESA SP-1200 (ESA/ESTEC, Noordwijk)

- Porter, J. M., & Rivinius, T. 2003, *PASP*, 115, 1153
- Rauw, G., & De Becker, M. 2004, *A&A*, 421, 693
- Reynolds, R. J., Sterling, N. C., & Haffner, L. M. 2001, *ApJ*, 558, L101
- Scargle, J. D. 1982, *ApJ*, 263, 835
- Seyfert, C. K., & Popper, D. M. 1941, *ApJ*, 93, 461
- Stickland, D. J., & Lloyd, C. 2001, *Observatory*, 121, 1
- Terebey, S., Fich, M., Taylor, R., Cao, Y., & Hancock, T. 2003, *ApJ*, 590, 906
- Townsend, R. H. D., Owocki, S. P., & Howarth, I. D. 2004, *MNRAS*, 350, 189
- Underhill, A. B. 1967, in *Determination of Radial Velocities and their Applications*, Proceedings IAU Symp. 30, ed. A. H. Batten & J. F. Heard (London: Academic Press), 167
- Underhill, A. B., & Gilroy, K. K. 1990, *ApJ*, 364, 626
- Van Hamme, W. 1993, *AJ*, 106, 2096
- Vasilevskis, S., Sanders, W. L., & van Altena, W. F. 1965, *AJ*, 70, 806
- Voroshilov, V. I., Guseva, N. G., Kalandadze, N. B., Kolesnik, L. N., & Kuznetsov, V. I. 1985, *Catalog of BV magnitudes and spectral classes of 6000 stars* (Kiev: Izdatel'stvo Naukova Dumka)
- Wade, R. A., & Rucinski, S. M. 1985, *A&AS*, 60, 471
- Walborn, N. R. 1972, *AJ*, 77, 312
- Walborn, N. R. 1973, *AJ*, 78, 1067
- Walborn, N. R. 2002, *AJ*, 124, 507
- Walborn, N. R., & Fitzpatrick, E. L. 1990, *PASP*, 102 379
- Walter, F. M. 1992, *PASP*, 104, 508
- Wilson, R. E. 1990, *ApJ*, 356, 613
- Wilson, R. E., & Devinney, E. J. 1971, *ApJ*, 166, 605



Table 1. Target Object Summary

Object Name	Spectral Class.	$\langle V_r \rangle^a$ (km s <sup>-1</sup> )	$\sigma(l-l)$ (km s <sup>-1</sup> )	$\sigma(s-s)$ (km s <sup>-1</sup> )	$\sigma$ (km s <sup>-1</sup> )	$T_{\text{eff}}$ (kK)	$\log g$ (cm s <sup>-2</sup> )	$V \sin i$ (km s <sup>-1</sup> )	Binary Status
DN Cas A	O8 V	-52	...	4.9	149.3	34.2	4.0	158 ± 20	SB2
DN Cas B	B0.2 V	-38	...	5.3	207.3	29.7	4.0	113 ± 18	SB2
BD+60°497 A	O6 V	-43	...	2.2	126.8	37.5	4.0	183 ± 9	SB2
BD+60°497 B	O8 V	-81	...	3.6	166.7	33.0	4.0	171 ± 19	SB2
BD+60°501	O6.5 V	-58	9.4	0.5	1.1	36.8	4.0	173 ± 10	constant
HD 15558	O5 III(f)	-49	5.3	1.8	2.9	39.5	3.7	195 ± 11	constant (SB1)
HD 15570	O4 If+	-55	0.9	0.8	4.2	42.9	3.5	123 ± 10	atmospheric var.
HD 15629	O5 V((f))	-60	8.1	1.2	2.2	41.5	4.0	106 ± 6	constant
BD+60°513	O7.5 Vn	-59	6.7	1.5	2.8	34.8	4.0	259 ± 5	constant
BD+62°424	O6.5 V((f))	-34	3.7	0.8	1.7	36.2	3.8	103 ± 12	constant
HD 17505 Aa1	O7.5 V((f))	-9	...	8.6	115.3	36.3	4.0	90 ± 10	SB2
HD 17505 Aa2	O7.5 V((f))	-44	...	7.2	118.2	36.5	4.0	120 ± 10	SB2
HD 17505 Ab	O6.5 III((f))	-38	8.2	...	...	37.5	3.8	80 ± 15	constant
HD 17520	O9 V	-54	2.7	0.7	6.0	33.2	4.0	80 ± 12	SB1 + Be
HD 237019	O8 V	-43	8.1	0.7	1.1	34.0	4.0	128 ± 5	constant
BD+60°586	O7.5 V	-48	4.7	1.0	1.0	35.4	4.0	95 ± 5	constant
BD+60°594	O8.5 Vn	-86	8.3	1.0	17.7	33.5	4.0	285 ± 16	SB1

<sup>a</sup>Systemic velocities for the binary stars are given in Tables 5, 7, and 9.

Table 2. Radial Velocity Measurements for Constant Velocity and SB1 Stars

Star Name	Date (HJD-2,450,000)	$V_r$ ( $\text{km s}^{-1}$ )
BD+60°501	2912.891	–56.6
BD+60°501	2912.968	–56.4
BD+60°501	2913.888	–57.2
BD+60°501	2913.965	–57.9
BD+60°501	2914.890	–57.4

Note. — Table 2 is published in its entirety in the electronic edition of the *Astrophysical Journal*. A portion is shown here for guidance regarding its form and content.

Table 3. Spectral Energy Distribution Fits

Object Name	Cluster Membership	$\theta_{LD}$ ( $10^{-6}$ arcsec)	$R_{\star}^a$ ( $R_{\odot}$ )	$E(B - V)$ (mag)	$R$ ( $A_V/E(B - V)$ )
DN Cas A ....	IC 1805	36 (1)	7.4 (7)	0.97 (1)	3.13 (1)
DN Cas B ....	IC 1805	26 (3)	5.3 (8)	0.97 (1)	3.13 (1)
BD+60°497 A	IC 1805	49 (4)	10.0 (13)	0.89 (2)	2.94 (6)
BD+60°497 B	IC 1805	32 (5)	6.5 (11)	0.89 (2)	2.94 (6)
BD+60°501 ..	IC 1805	36 (3)	7.2 (9)	0.76 (2)	3.12 (5)
HD 15558 A ..	IC 1805	81 (10)	16.4 (26)	0.84 (3)	3.07 (9)
HD 15558 B ..	IC 1805	28 (4)	5.6 (9)	0.84 (3)	3.07 (9)
HD 15570 ....	IC 1805	95 (16)	19.3 (37)	1.01 (2)	3.13 (7)
HD 15629 ....	IC 1805	57 (7)	11.6 (19)	0.76 (3)	3.09 (12)
BD+60°513 ..	IC 1805	43 (4)	8.7 (12)	0.83 (3)	3.00 (5)
BD+62°424 ..	IC 1805	49 (3)	9.9 (11)	0.75 (2)	3.02 (4)
HD 17505 Ab .	IC 1848	56 (6)	11.4 (16)	0.72 (3)	2.83 (9)
HD 17505 Aa1	IC 1848	49 (8)	10.0 (18)	0.72 (3)	2.83 (9)
HD 17505 Aa2	IC 1848	49 (8)	10.0 (18)	0.72 (3)	2.83 (9)
HD 17505 B ..	IC 1848	44 (6)	8.9 (15)	0.72 (3)	2.83 (9)
HD 17520 Aa .	IC 1848	38 (11)	7.7 (24)	0.57 (5)	3.10 (120)
HD 17520 Ab .	IC 1848	14 (4)	2.8 (9)	0.57 (5)	3.10 (120)
HD 17520 B ..	IC 1848	34 (10)	7.0 (22)	0.57 (5)	3.10 (120)
HD 17520 C ..	IC 1848	14 (4)	2.8 (9)	0.57 (5)	3.10 (120)
HD 237019 ...	IC 1848	37 (1)	7.4 (7)	0.77 (1)	3.20 (6)
BD+60°586 A	IC 1848	45 (3)	9.1 (11)	0.58 (3)	3.27 (32)
BD+60°586 B	IC 1848	25 (2)	5.1 (7)	0.58 (3)	3.27 (32)
BD+60°594 A	IC 1848	35 (4)	7.2 (11)	0.68 (2)	2.88 (10)
BD+60°594 B	IC 1848	10 (2)	2.0 (5)	0.68 (2)	2.88 (10)

<sup>a</sup>Radius derived for a distance of 1.886 kpc.

Table 4. Radial Velocity Measurements for DN Cas

Date (HJD-2,450,000)	Orbital Phase	$V_1$ (km s <sup>-1</sup> )	$(O - C)_1$ (km s <sup>-1</sup> )	$V_2$ (km s <sup>-1</sup> )	$(O - C)_2$ (km s <sup>-1</sup> )
2912.849	0.814	143.9	-1.4	-318.3	-7.1
2912.932	0.850	118.0	-3.8	-282.5	-3.8
2913.003	0.881	99.4	4.6	-238.3	2.9
2913.825	0.237	-255.4	2.7	244.1	-4.2
2913.834	0.241	-257.6	0.8	245.4	-3.4
2913.839	0.243	-259.7	-1.1	247.4	-1.6
2913.844	0.245	-256.1	2.6	246.6	-2.5
2913.927	0.281	-255.9	-1.0	241.1	-2.7
2914.004	0.314	-241.9	0.1	221.2	-4.7
2914.814	0.665	133.1	0.4	-297.8	-4.0
2914.943	0.721	154.9	-3.7	-337.5	-7.7
2915.025	0.756	154.1	-8.0	-352.3	-17.8
2915.656	0.029	-109.8	-23.1	4.7	-5.9
2915.883	0.127	-200.8	-1.5	161.9	-4.8
2915.931	0.148	-221.7	-4.6	182.5	-9.0
2916.015	0.184	-239.8	1.4	229.9	5.1
2916.747	0.501	-59.8	-13.1	-47.3	-2.4
2916.756	0.505	-31.6	10.1	-82.0	-30.1
2916.792	0.521	-17.3	3.4	-66.2	14.7
2916.797	0.523	-14.6	3.6	-56.4	28.2
2916.805	0.526	-10.9	3.0	-55.6	34.9
2916.809	0.528	-18.8	-7.5	-59.1	35.1
2916.818	0.532	3.7	10.3	-102.2	-1.6
2916.822	0.534	8.7	12.6	-98.6	5.7
2916.846	0.544	17.7	8.4	-123.8	-1.1
2916.851	0.546	14.4	2.5	-128.6	-2.3
2916.943	0.586	64.2	4.3	-195.9	-3.2
2917.018	0.618	92.2	-1.9	-247.1	-6.8

Table 5. Orbital Elements for DN Cas

Element	Value
$P$ (days) .....	2.310950 (2)
$T_{\min}$ (HJD-2,450,000)	2915.579 (2)
$e$ .....	0
$\omega$ ( $^{\circ}$ ) .....	...
$K_1$ (km s $^{-1}$ ) .....	210.5 (20)
$K_2$ (km s $^{-1}$ ) .....	292.0 (38)
$M_2/M_1$ .....	0.721 (12)
$\gamma$ (km s $^{-1}$ ) .....	-48.3 (14)
$\gamma$ (km s $^{-1}$ ) .....	-42.7 (27)
$i$ ( $^{\circ}$ ) .....	79.2 (11)
$M_1$ ( $M_{\odot}$ ) .....	19.2 (8)
$M_2$ ( $M_{\odot}$ ) .....	13.9 (5)
$R_1$ ( $R_{\odot}$ ) .....	7.4 (6)
$R_2$ ( $R_{\odot}$ ) .....	5.4 (8)
$R_1/R_1(\text{lobe})$ .....	0.78 (6)
$R_2/R_2(\text{lobe})$ .....	0.66 (10)
$a$ ( $R_{\odot}$ ) .....	23.3 (2)
r.m.s. $_1$ (km s $^{-1}$ ) .....	7.4
r.m.s. $_2$ (km s $^{-1}$ ) .....	14.1

Note. — Numbers in parentheses give the error in the last digit quoted.

Table 6. Radial Velocity Measurements for BD+60°497

Date (HJD-2,450,000)	Orbital Phase	$V_1$ (km s <sup>-1</sup> )	$(O - C)_1$ (km s <sup>-1</sup> )	$V_2$ (km s <sup>-1</sup> )	$(O - C)_2$ (km s <sup>-1</sup> )
2912.871	0.151	-214.8	0.6	136.3	-6.1
2912.953	0.171	-224.3	-6.5	145.4	-0.1
2913.874	0.404	-100.0	2.7	30.7	34.7
2913.946	0.422	-66.7	22.4	-18.9	2.7
2914.823	0.644	70.7	8.0	-216.0	2.7
2914.826	0.644	65.0	2.0	-217.6	1.7
2914.832	0.646	63.6	-0.3	-217.5	2.9
2914.836	0.647	60.1	-4.3	-230.5	-9.5
2914.844	0.649	64.5	-0.9	-220.8	1.4
2914.848	0.650	68.6	2.6	-222.9	0.2
2914.857	0.652	69.8	2.6	-219.4	5.1
2914.862	0.654	63.9	-3.8	-228.9	-3.6
2914.965	0.680	74.6	-5.4	-238.0	3.1
2915.825	0.897	41.3	-3.9	-194.0	1.9
2915.829	0.898	39.8	-4.4	-197.5	-2.8
2915.833	0.899	36.6	-6.6	-198.4	-5.0
2915.842	0.901	38.9	-2.0	-191.8	-1.3
2915.846	0.902	38.0	-2.0	-194.2	-5.0
2915.952	0.929	16.9	6.6	-169.0	-18.3
2916.831	0.151	-210.9	4.6	142.0	-0.5
2916.835	0.152	-206.3	9.3	148.4	5.7
2916.859	0.158	-214.1	2.5	139.0	-5.0
2916.863	0.159	-216.2	0.6	145.6	1.4
2916.932	0.176	-212.9	5.0	139.0	-6.7
2917.011	0.196	-219.1	-2.8	132.5	-11.1

Table 7. Orbital Elements for BD+60°497

Element	Rauw & De Becker (2004)	This paper
$P$ (days) .....	3.96 (9)	3.95863 (21)
$T$ (HJD-2,450,000)	...	2916.233 (15)
$T_0$ (HJD-2,450,000)	2935.98 (15)	...
$e$ .....	0	0.156 (19)
$\omega$ ( $^\circ$ ) .....	...	100 (11)
$K_1$ (km s $^{-1}$ ) .....	172 (12)	159.9 (22)
$K_2$ (km s $^{-1}$ ) .....	221 (15)	207.7 (29)
$M_2/M_1$ .....	0.78 (8)	0.770 (15)
$\gamma_1$ (km s $^{-1}$ ) .....	−54 (9)	−53.8 (17)
$\gamma_2$ (km s $^{-1}$ ) .....	−69 (12)	−67.5 (23)
$M_1 \sin^3 i$ ( $M_\odot$ ) .....	13.9 (25)	11.1 (5)
$M_2 \sin^3 i$ ( $M_\odot$ ) .....	10.9 (20)	8.6 (4)
$a \sin i$ ( $R_\odot$ ) .....	30.7 (19)	28.39 (28)
r.m.s. $_1$ (km s $^{-1}$ ) ...	...	10.9
r.m.s. $_2$ (km s $^{-1}$ ) ...	...	14.4

Note. — Numbers in parentheses give the error in the last digit quoted.

Table 8. Radial Velocity Measurements for HD 17505Aa

HJD (-2,450,000)	Orbital Phase	$V_1$ (km s <sup>-1</sup> )	$(O - C)_1$ (km s <sup>-1</sup> )	$V_2$ (km s <sup>-1</sup> )	$(O - C)_2$ (km s <sup>-1</sup> )
1817.887	0.772	-181.1	5.3	143.7	5.2
1818.890	0.889	-184.6	-2.8	136.3	2.6
1819.873	0.004	-77.9	-1.3	18.9	-6.9
1820.887	0.122	63.4	-0.2	-124.7	-6.7
1821.864	0.236	148.2	15.8	-190.4	-1.9
1822.865	0.353	120.9	3.7	-171.9	1.1
1823.814	0.464	49.2	0.0	-105.9	-2.9
1823.924	0.476	35.7	-3.4	-95.7	-2.8
1824.825	0.582	-45.5	4.8	1.0	2.0
1824.950	0.596	-54.8	8.4	16.6	4.5
1830.842	0.284	142.9	7.5	-187.7	3.8
1830.946	0.296	136.5	2.5	-180.0	10.1
1888.797	0.045	-29.1	-4.5	-34.0	-6.5
1889.746	0.156	91.2	-2.1	-148.5	-0.0
1892.743	0.506	...	...	...	...
1893.774	0.626	-77.2	11.8	25.5	-13.0
1894.771	0.742	-168.5	4.5	131.3	6.6
1894.845	0.751	-183.3	-6.0	136.3	7.2
1895.721	0.853	-196.3	-1.8	144.7	-2.1
1895.811	0.864	-184.3	7.5	144.7	0.6
1896.651	0.962	-132.7	-8.0	76.7	1.4
1896.784	0.977	-103.8	4.1	45.3	-12.6
1897.652	0.078	6.0	-10.1	-71.1	-1.8
1897.784	0.094	21.0	-12.9	-87.4	0.1
1898.656	0.196	114.5	-3.8	-177.2	-3.2
1898.793	0.212	126.0	0.8	-173.9	7.2
1899.658	0.312	133.2	2.5	-182.4	4.3
1899.791	0.328	124.9	-1.5	-182.2	0.2
1900.653	0.429	69.7	-4.9	-136.9	-7.7
1900.784	0.444	60.6	-3.2	-124.9	-6.7
1901.637	0.543	-32.7	-15.8	-14.1	21.2
1901.770	0.559	-27.6	3.0	-24.4	-3.0

Table 9. Orbital Elements for HD 17505Aa

Element	Value
$P$ (days) .....	8.5710 (8)
$T$ (HJD-2,450,000)	1862.696 (16)
$e$ .....	0.095 (11)
$\omega$ ( $^\circ$ ) .....	252 (6)
$K_1$ ( $\text{km s}^{-1}$ ) .....	166.5 (18)
$K_2$ ( $\text{km s}^{-1}$ ) .....	170.8 (18)
$M_2/M_1$ .....	0.975 (15)
$\gamma_1$ ( $\text{km s}^{-1}$ ) .....	-25.8 (12)
$\gamma_2$ ( $\text{km s}^{-1}$ ) .....	-26.3 (12)
$M_1 \sin^3 i$ ( $M_\odot$ ).....	17.1 (6)
$M_2 \sin^3 i$ ( $M_\odot$ ).....	16.6 (6)
$a \sin i$ ( $R_\odot$ ) .....	56.8 (4)
r.m.s. <sub>1</sub> ( $\text{km s}^{-1}$ ) ..	7.0
r.m.s. <sub>2</sub> ( $\text{km s}^{-1}$ ) ..	7.0

Note. — Numbers in parentheses give the error in the last digit quoted.

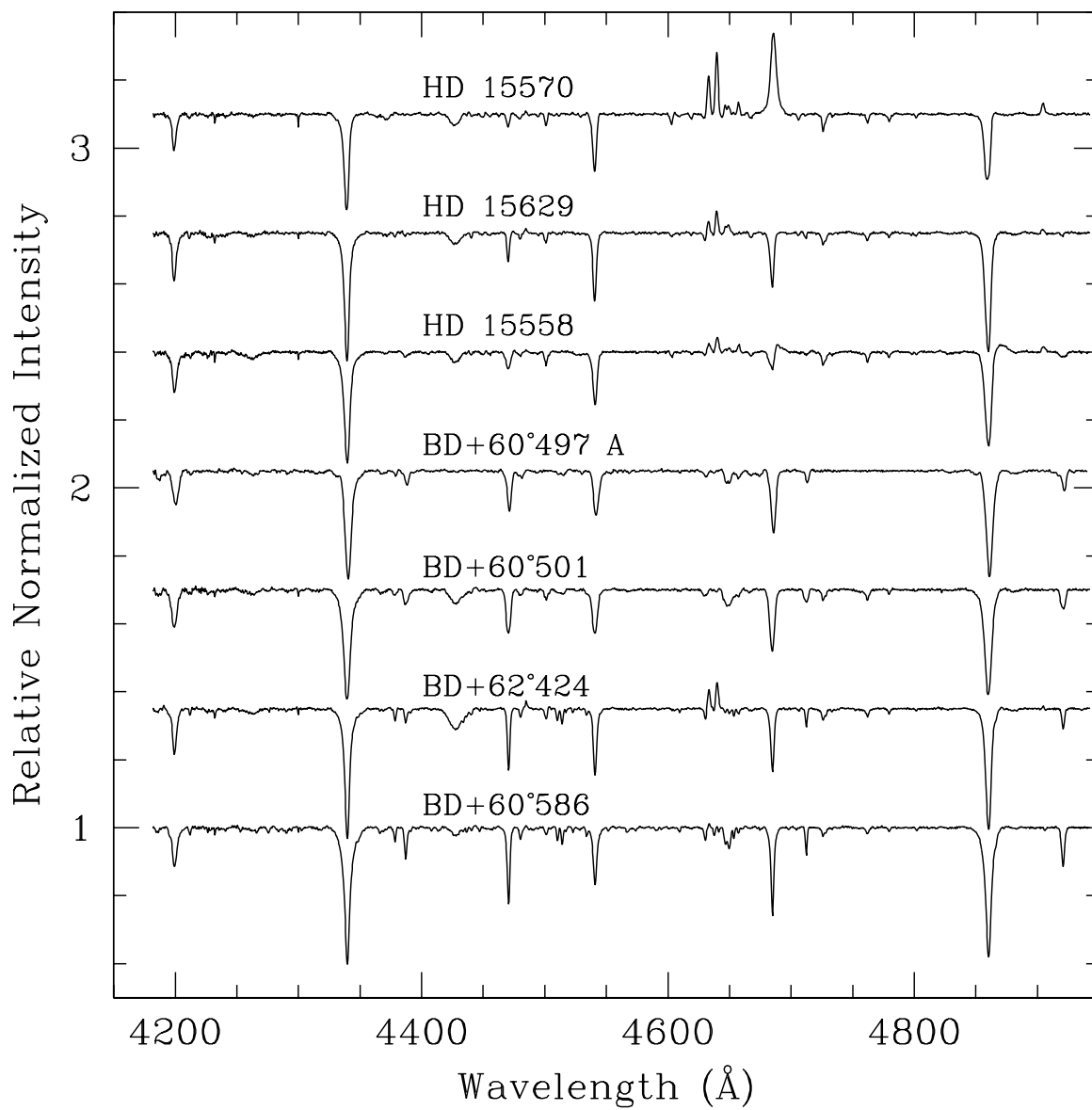


Fig. 1.— The observed mean spectra sorted by temperature. Here we show the seven hottest stars with the hottest at the top. The spectra have been continuum normalized and shifted vertically for clarity. Note that interstellar features (such as the 4428 Å diffuse interstellar band) are cut out of the tomographic reconstructions but are present in the other spectra.

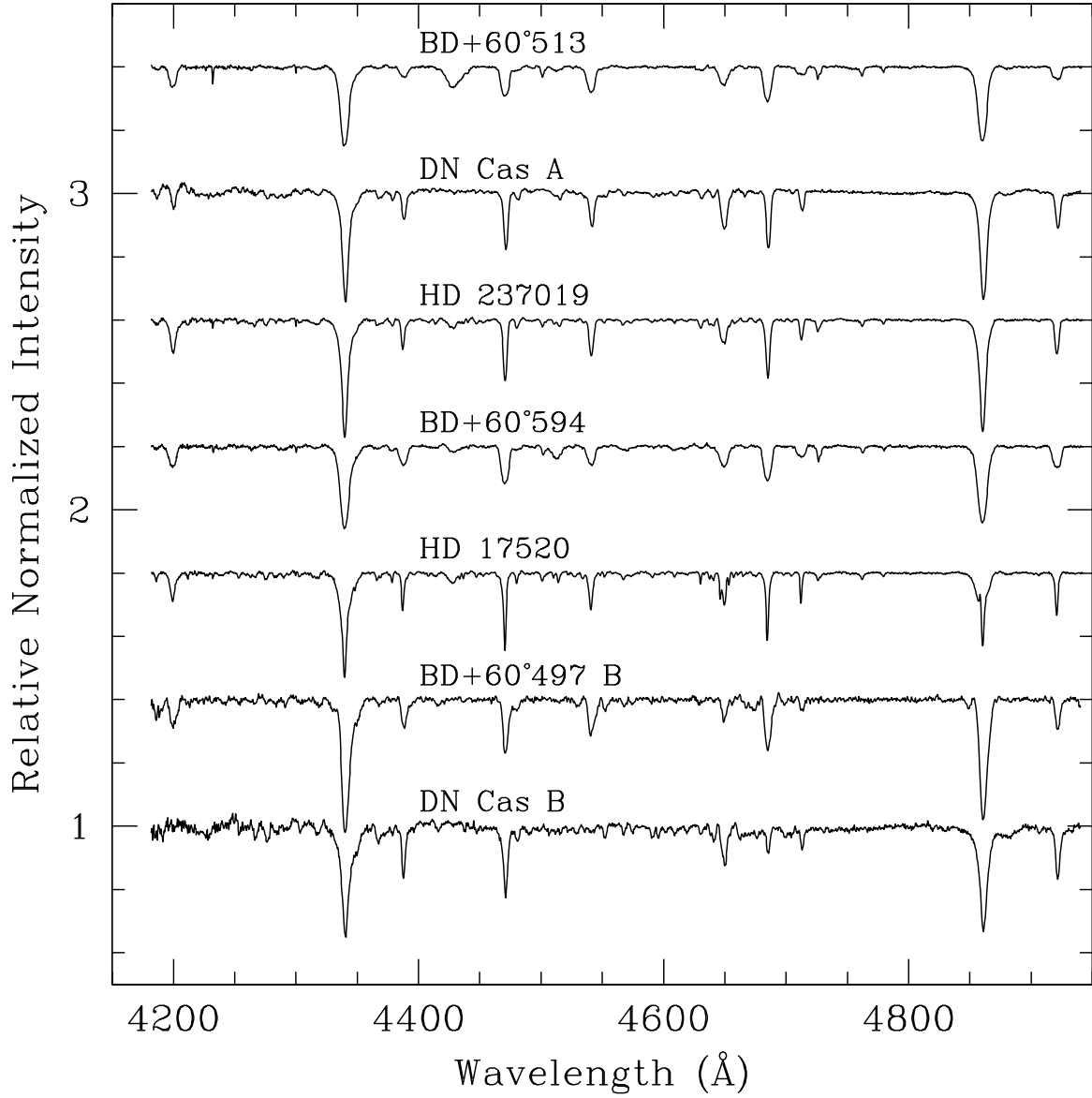


Fig. 2.— The observed spectra sorted by temperature. Here we show the seven coolest stars with the coolest at the bottom. The spectra have been continuum normalized and shifted vertically for clarity.

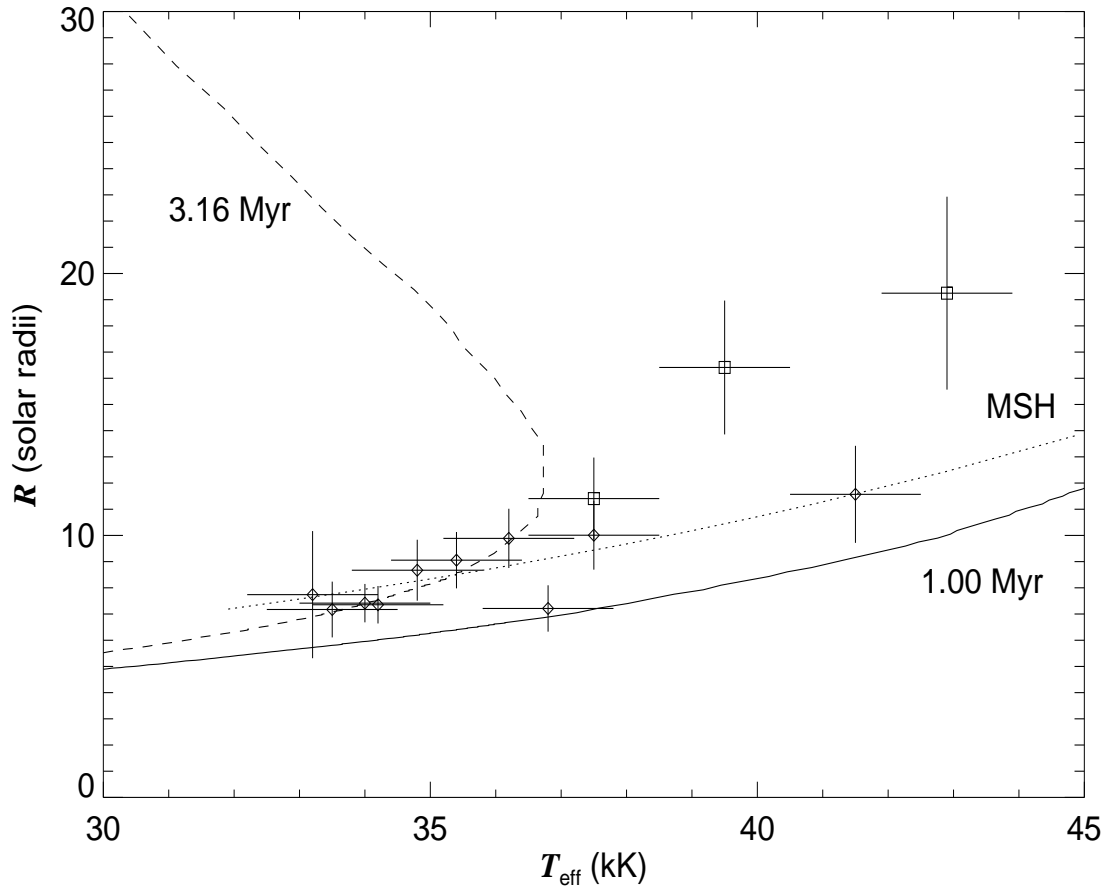


Fig. 3.— The stellar radii (for an assumed distance of 1.9 kpc) plotted versus effective temperature (*diamonds* = V, *squares* = I, III luminosity classes). The solid and dashed lines show the predicted radii for ages of 1.00 and 3.16 Myr, respectively (Lejeune & Schaerer 2001). The dotted line indicates the relationship given for main sequence stars by Martins et al. (2005) (see their Table 4).

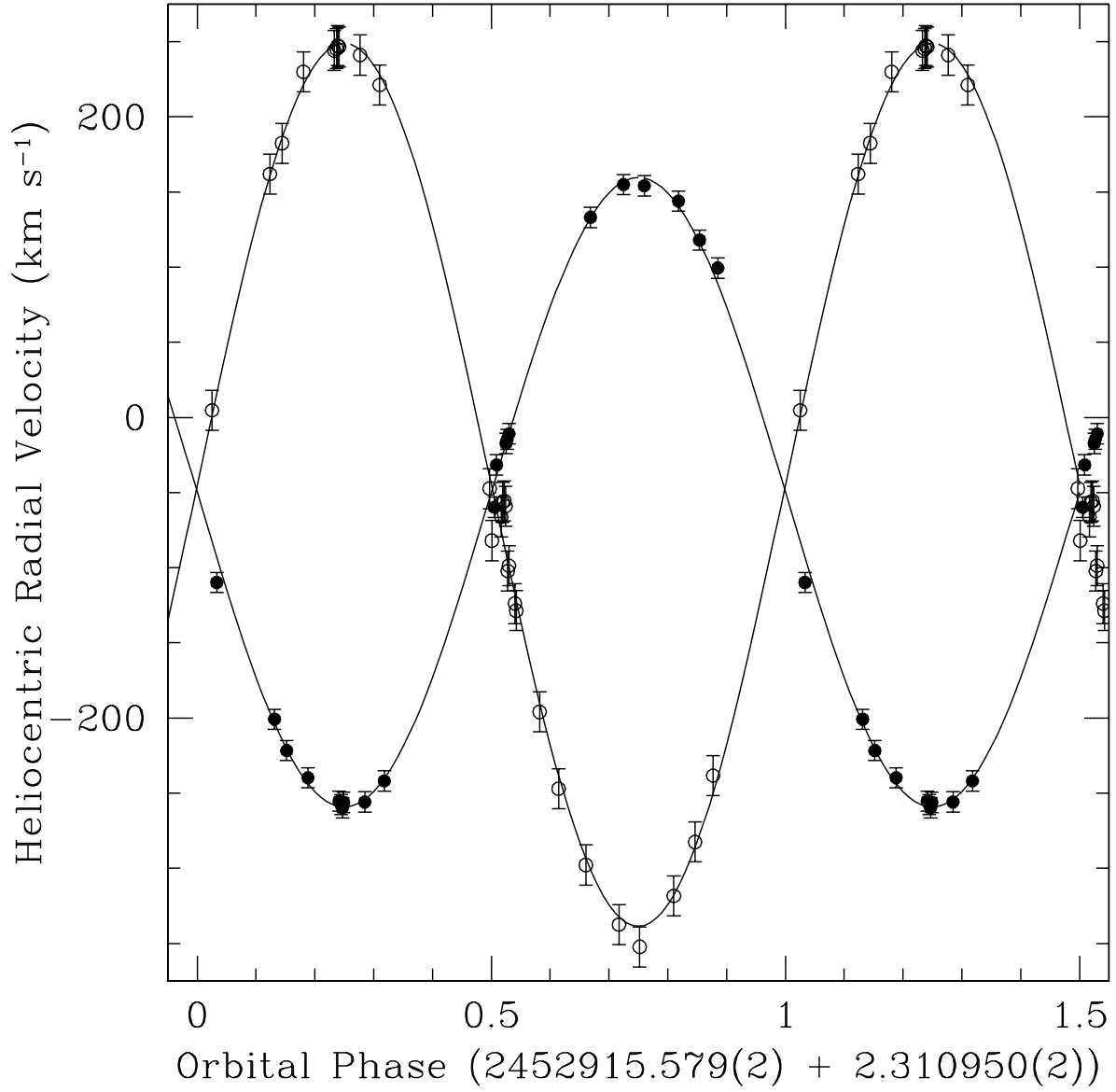


Fig. 4.— The DN Cas radial velocity data folded on the given ephemeris and plotted with the calculated orbital velocity curves.

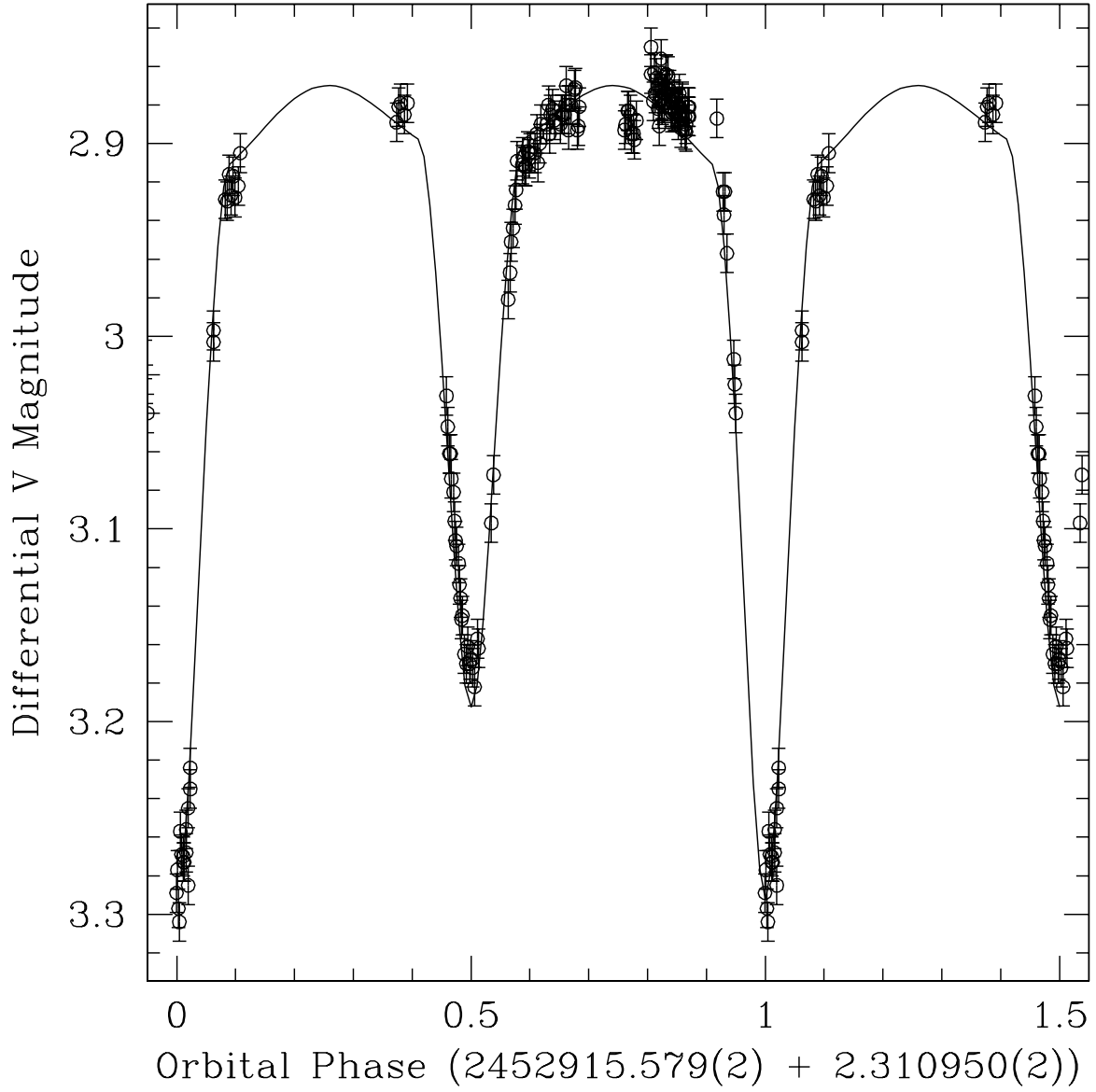


Fig. 5.— The DN Cas *V*-band photometry data folded on the given ephemeris and plotted with the Wilson-Devinney code light curve.

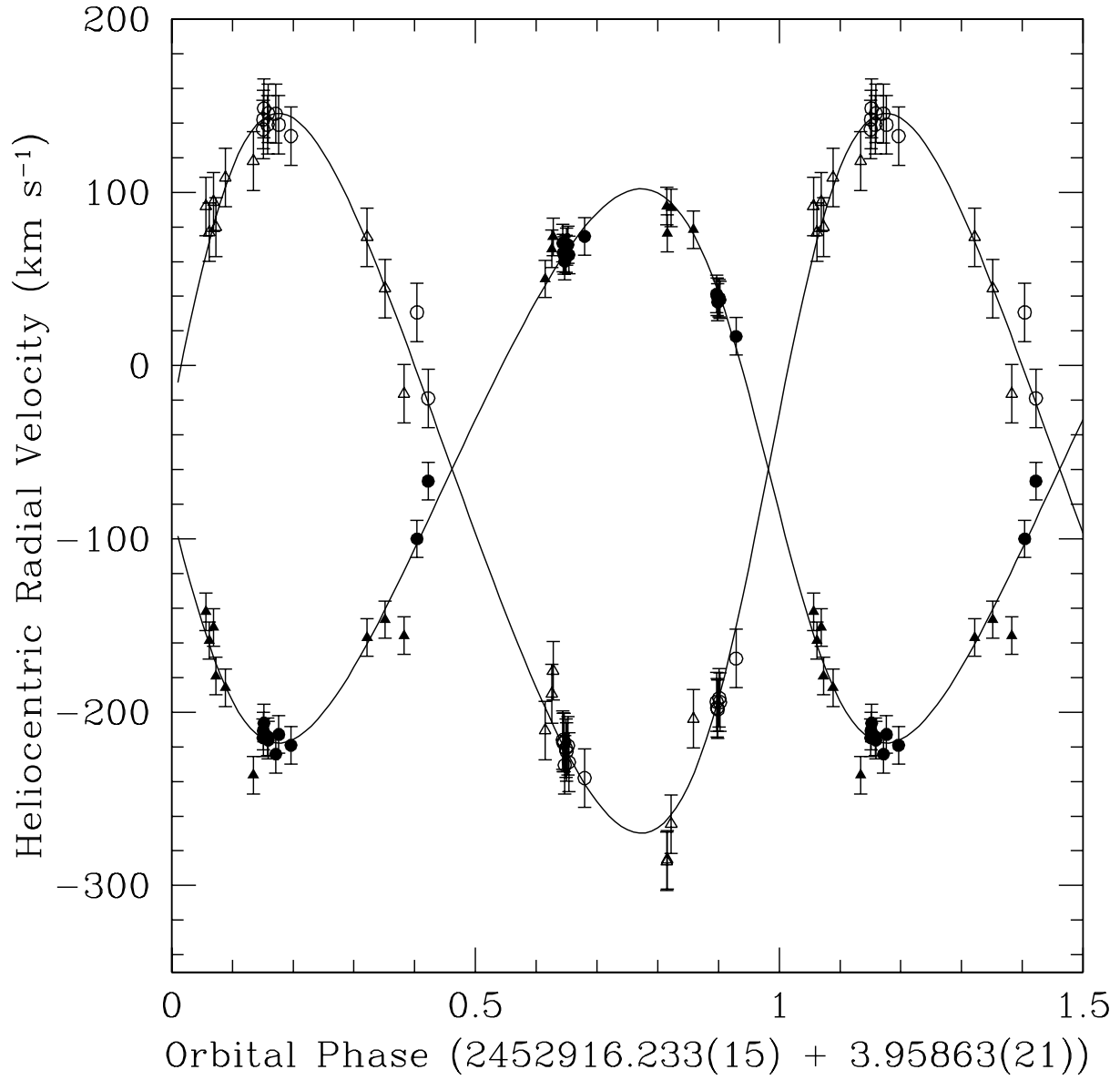


Fig. 6.— Our radial velocity data (*circles*) with the data from Rauw & De Becker (2004) (*triangles*) for BD+60°497. The data is folded on the given ephemeris and plotted with the calculated model (*line*). The solid points denote radial velocities of the primary and the open points represent secondary star velocities.

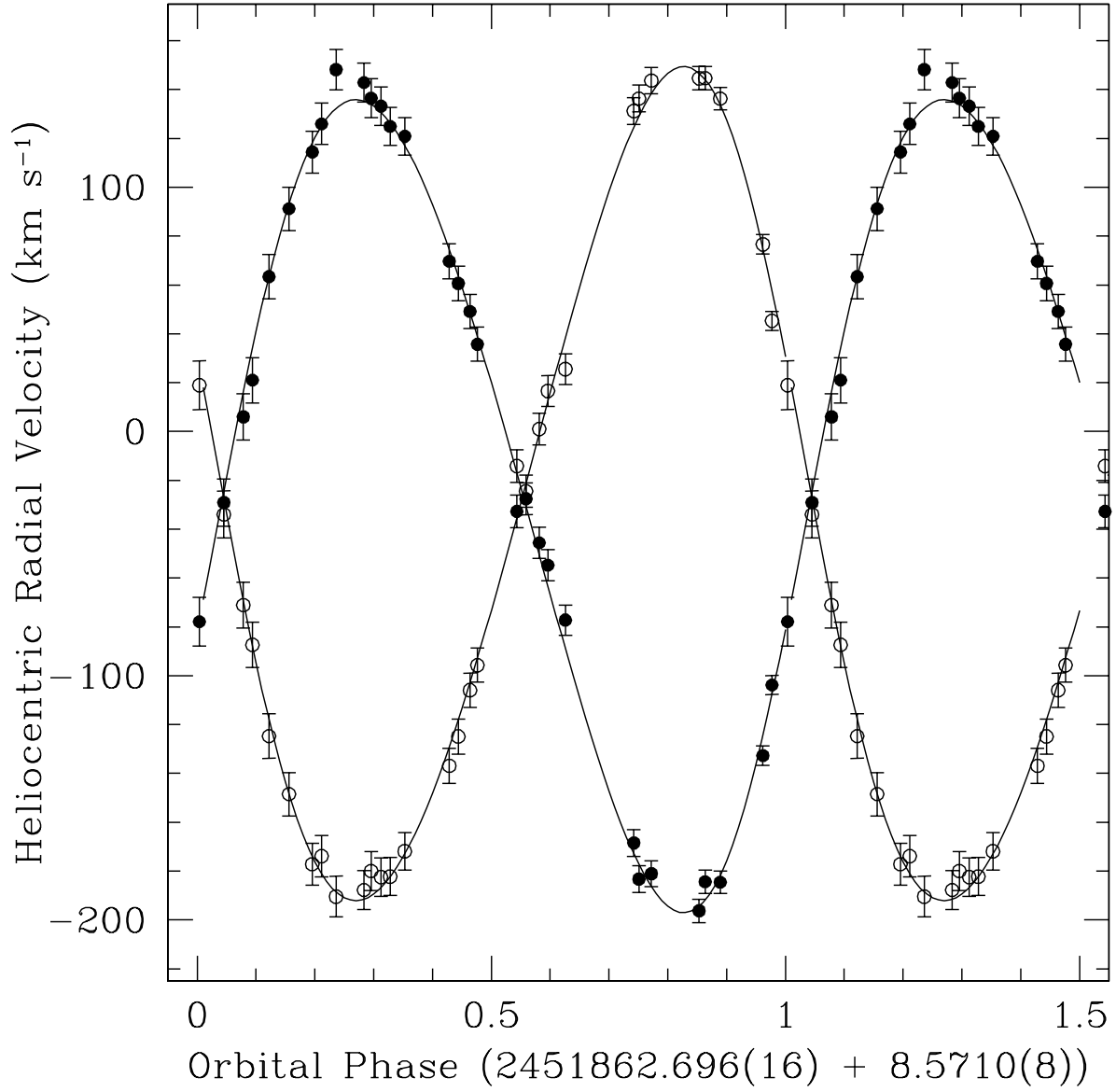


Fig. 7.— The HD 17505Aa radial velocity data folded on the given ephemeris, plotted with the calculated radial velocity curve.

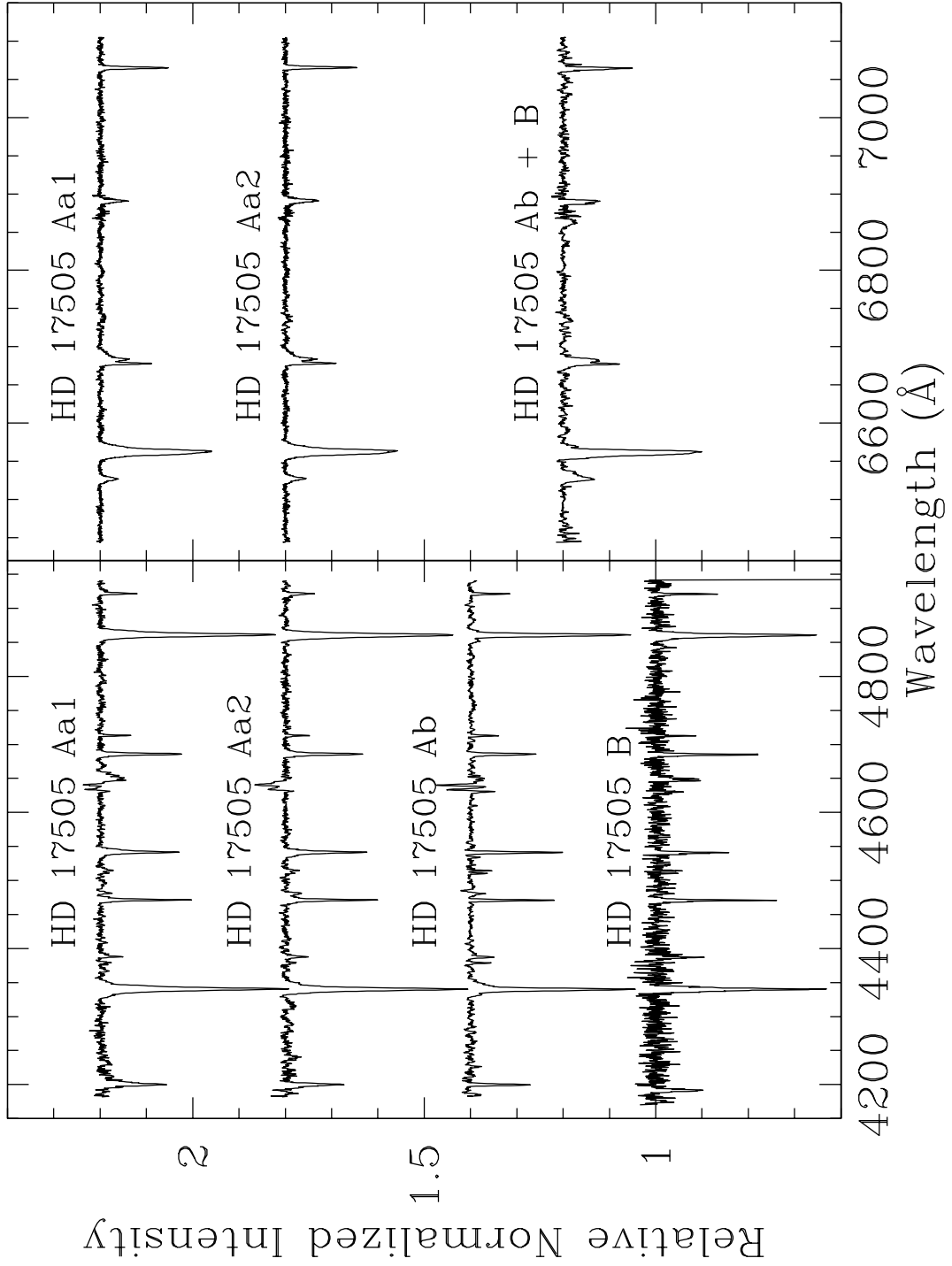


Fig. 8.— Spectra for the components of HD 17505 in both the blue and red wavelength regions.

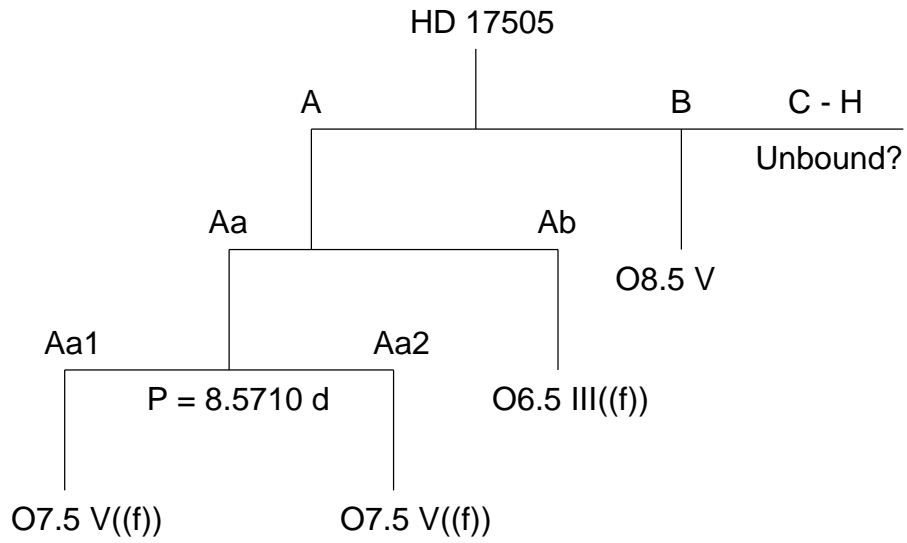


Fig. 9.— Diagram showing the hierarchy of the HD 17505 system.